LEX LOCALIS-JOURNAL OF LOCAL SELF-GOVERNMENT
ISSN:1581-5374 E-ISSN:1855-363X
VOL. 22, NO. 4(2024)

INTELLIGENT LAND COVER CLASSIFICATION AND ROUTE PLANNINGUSING HYPERSPECTRAL-LIDAR FUSION AND OPTIMIZER

Ms. Priti Nahar[1], Dr. Sushant Kumar[2], Dr. Anupam Shukla[3]

[1]Indian Institute of Information Technology, Pune,
[2]Indian Institute of Information Technology, Pune
[3]SVNIT, Surat

Abstract
The proper location of transmission lines is critical for optimising energy distribution while minimising environmental damage. This research seeks to improve the identification of potential places for transmission line placement by using sophisticated classification algorithms, notably Convolutional Neural Networks (CNNs) based on hyperspectral and LiDAR data.
We used a comprehensive strategy that included several remote sensing technologies to properly categorize land cover types and provide a binarized picture showing potential installation locations. The system featured a rigorous CNN-based categorisation procedure, followed by optimum route selection for transmission line routing, which ensured environmental compliance.
Our findings show good classification accuracy across a variety of land cover categories, with particularly strong performance in "Trees," "Road," and "Water," with accuracy rates of 98%, 95%, and 97%. The misclassification rates were also analyzed, giving information for future model modification. The resulting visualizations clearly depict the ideal transmission line pathways, demonstrating the model's trustworthiness.
In conclusion, this research effectively creates a robust framework for transmission line planning that uses CNNs and remote sensing data to deliver actionable insights, therefore contributing to long-term infrastructure development.

Keywords: LiDAR image, HyperSpectral image, CNN, Transmission Line, optimal path, landcover.

1 Introduction

Power infrastructure is a vital component of the country's economy and the livelihood of its citizens. If the power infrastructure fails, significant financial losses will result. As a result, the state invests a significant amount of money and labour in inspection work each year[1]. Pylons and transmission cables are expanding quickly in tandem with the economy. Transmission lines must reach hostile locations, which are typically isolated and complex, including rough mountains. This necessitates challenging inspection work[2]. However, in order to increase transmission capacity, the power industry must employ numerous compact towers with multiple loops. This leads to a large deal of complexity in power line distribution and mutual inductance, which makes fault detection and ranging extremely challenging [3]. These new issues are placing pressure on inspection capabilities to develop an efficient autonomous inspection approach that makes use of the equipment already in place in order to decrease labour costs and inspection errors while increasing inspection efficiency. Consequently, research on autonomous inspection techniques is extremely important from a practical standpoint [4].
The purpose of transmission line inspection is to evaluate a transmission line's operating state and identify any potential issues [5]. Long-term exposure to extreme weather conditions, such as significant temperature differences, excessive humidity, and encroaching vegetation, can result in a variety of flaws, including damper slippage, broken strands, and electrical flashovers, which can cause widespread blackouts or even forest fires [6]. As a result, monitoring how fittings,

cables, and the environment affect gearbox lines is a crucial part of gearbox line inspection. Currently, there are four basic categories into which inspection methods can be placed: robot inspection, airborne inspection, vehicle inspection, and manual inspection [7].

Manual inspection is the process of using a telescope or the unaided eye to observe electricity wires and their surroundings. This approach is expensive, time-consuming, labour-intensive, and imprecise. Certain power line segments that are impacted by terrain cannot be inspected because they are located in difficult-to-access places for inspection staff and vehicles. As a result, efforts are made to create a wide range of sophisticated inspection techniques to replace manual inspection. But as of right now, manual inspection remains the most used inspection technique [8].

In order to perform inspection operations along a power line, vehicle inspection uses a vehicle as a carrying platform equipped with integrated GPS, INS, laser scanner, cameras, and other sensors[9]. Because vehicles can be equipped with sizable, high-power inspection tools to perform precision inspection duties, vehicle inspection is more versatile [10]. Unfortunately, this technique is only applicable to city power line inspections[11].

Aircraft are used as the carrying platform for airborne inspections; these aircraft are mostly of three types: fixed-wing UAVs, multirotor UAVs, and helicopters. Among these, helicopter inspection is a productive technique for inspection that is not location-specific and can do inspection jobs fast without interfering with power transmission [12]. Nonetheless, the intricate operating environment has a significant impact on helicopters. For instance, in metropolitan settings, a lot of buildings are taller than a helicopter's scanning height, making it challenging to do high-quality inspections close to gearbox lines. As a result, this inspection technique is dangerous, expensive, and weather-dependent. It is currently extensively utilised in ultra-high-voltage gearbox line inspection jobs [13]. Fixed-wing UAV inspection is less expensive than helicopter inspection. Low accuracy, a high technical threshold, and a lengthy process for a large-scale inspection work are the drawbacks of fixed-wing UAV inspection, albeit [14]. Excellent flight stability and suspension capabilities make multirotor UAVs ideal for point-to-point HD video capture and real-time observation on power lines. Nevertheless, the multirotor UAV's load capacity is restricted, and simultaneously carrying multiple inspection instruments is a challenging task. Its use has been restricted to long-distance inspection due to its brief duration [15].

A cable inspection robot is used as a motion platform for robot inspection. It can be separated into CIR inspection and substation robot inspection based on various inspection objects. When performing substation inspection work, robot inspection takes the place of hand inspection [16]. Because CIR is a power robot that travels along a ground wire, it can access difficult-to-reach areas like mountains, woods, and lakes and perform fine inspection there[17]. CIR has a certain amount of load capacity and can be fitted with inspection tools. In certain difficult circumstances, CIR may also replenish power online through solar charging or downhill-generated electricity [24]. This makes it appropriate for automated inspection.

Three autonomous aspects—autonomous operation, autonomous target inspection, and autonomous positioning inspection—are the three fundamental components of autonomous inspection in this work. The basis of other autonomous applications is autonomous operation, which is the capacity to autonomously choose a motion path and automatically modify movement in accordance with path planning to reach different places required by gearbox line inspection[18]. The capacity to automatically identify inspection targets or locations in

accordance with task planning is known as autonomous target inspection [19]. Automatic positioning inspection gathers positional data and autonomously identifies issues at predetermined points.

In recent years, Light Detection and Ranging (LiDAR) technology has become an indispensable tool in power line inspections, offering key improvements in data acquisition[20]. According to[21], LiDAR devices are active sensors that measure the separation between an object or the ground using a laser emissor. They fall into two categories: discrete sensors, which only record a limited number of returns, and waveform sensors, which provide the entire laser return. The device determines how many returns there will be.

LiDAR data is typically displayed as point clouds, which are collections of points that are typically represented in LAS files. Each point in the cloud has a laser return, a position, and an intensity value at the very least. Certain sensors also provide additional information about each point, such as the RGB values or a date.

2 Related work

Proposed an automatic clearance anomaly detection method using LiDAR point clouds[22]. The method efficiently and flexibly detects clearance hazards, such as tree encroachment, by measuring the distance between power lines and non-power-facility objects in the Right-of-Ways (ROW) corridor. The method's effectiveness and accuracy were validated through qualitative visual inspection, quantitative manual measurements, and on-site field surveys.A novel UAV inspection system has been developed by [23]to address challenges in control model and ground clearance measurement in transmission line corridors. The system uses a dual-view stereovision module and an advanced embedded NVIDIA platform, with advanced algorithms for autonomous control and ground clearance measurement. Tests show the system can be applied in practical inspection environments and performs well.Introduces a power line corridor inspection method using UAV LiDAR edge computing and 4G real-time transmission[24]. It classifies power towers into various types, analyzes spatial and topological relations, and promptly notifies maintenance personnel of potential risks.

According to [25] power lines are becoming more complex and difficult to inspect, requiring advanced LiDAR technology. A novel methodology using cable inspection robot (CIR) LiDAR data and POS data is proposed to detect inspection objects surrounding power lines. The method achieves an average accuracy of 90.6% and precision of 98.2%.[26]presents a new method for automatic wire extraction from power line corridors using LiDAR point cloud data. The method removes pylon and vegetation points, extracts wire points, divides spans, uses clustering algorithms, and separates wires. Experimental results show 99% completeness and 100% correctness.Presented a method for extracting and classifying 3D targets of electric power transmission facilities using point cloud data from unmanned aerial vehicles[27]. The method achieves 97% precision and eliminates interference, providing valuable 3D geo-information for UAV remote-sensing inspection and corridor safety maintenance.

As per [28] traditional inspection methods have limitations like high labor intensity and long re-inspections. Airborne LiDAR can provide high-precision spatial information for transmission line inspection, accurately detecting dangerous points. The grid method divides data into regions for elevation histogram statistical method.An algorithm to automatically detect power transmission lines (PTLs)' wires and pylons using UAV LiDAR data. The algorithm analyzes safety distances and detects risky ground objects. The algorithm achieves high accuracy and

quality values for wires and pylons, making periodic monitoring easier without time-consuming fieldwork[29].A UAV system using advanced embedded processors and binocular visual sensors to generate real-time guidance information for automatic transmission line inspection. The system uses a convolutional neural network to detect power lines with different pixel widths and orientations, outperforming other methods in experimental results[30]. Airborne LiDAR surveying and mapping technology for transmission line engineering surveys, generating high-precision surface DEM and extracting single wood information for accurate tree felling count[31].

3 Background

3.1 LiDAR

The laser ranging system, the dynamic differential measuring system, the inertial measurement device, the imaging device, and other components make up the multi-sensor airborne LiDAR measurement system.Since the speed of light is known, the propagation time can be converted to distance; that is, the mode of the vector is the distance between the transmitter and the ground laser foot as measured by the laser ranging system. This is accomplished by using a laser pulse rangefinder mounted on a UAV platform to transmit a discrete laser pulse through the air to the surface of the terrain or ground object, which is reflected back through the surface and received by the receiver. This allows for an accurate measurement of the light pulse from the emission to the interval between reflections [32].The flying platform's exact position is provided by dynamic differential GNSS, and its attitude parameters—such as roll, tilt, and heading angles—are measured in space by inertial measurement of a single cloud (IMU).

By employing an encoder and inertial navigation system to get four azimuths of aircraft in flight, the airborne LiDAR can determine the position of a laser foot on the ground using the principle of space geometric vector placement.The laser scanner uses dynamic differential DGPS to determine the distance between the ground point and the center of the laser scanner. This allows the calculation of the other end of the laser vector by obtaining the coordinates of the starting point, which is the laser scanner center$O_s(X_sY_sZ_s)$. Points $P(XYZ)$ three-dimensional coordinates are as follows. The idea that aerial LiDAR devices can determine a ground foot's location is seen in Figure 1. Multiple reflections of the same pulse, such as a laser pulse striking a tree crown first, with a portion of it continuing to strike the leaves or branches below, or continuing to strike the ground below, can be captured by the onboard LiDAR measurement system. In order to gather all three-dimensional feature information fully, several return point records will be produced [33].Formula (1) displays the calculating formula.

$$\begin{cases} X_i = X_0 + \Delta X_i = X_0 + f_x(\varphi, \omega, k, \theta, s) \\ Y_i = Y_0 + \Delta Y_i = Y_0 + f_y(\varphi, \omega, k, \theta, s) \\ Z_i = Z_0 + \Delta Z_i = Z_0 + f_Z(\varphi, \omega, k, \theta, s) \end{cases} \quad (1)$$

Here:

- X_0, Y_0, Z_0 are the initial coordinates of the laser scanner center.
- φ, ω, k are the roll, pitch, and yaw angles of the aircraft or LiDAR platform, which determine the orientation in space.
- θ is the angle of the laser pulse relative to the scanner's orientation.
- s is the distance or range from the laser scanner to the target point on the ground.
- f_x, f_yandf_Z are the functions that compute the changes in each axis ($\Delta X_i, \Delta Y_i, \Delta Z_i$) based on these parameters.

Both the positional and angular modifications required to precisely pinpoint a ground point using the LiDAR data are incorporated into these transformations.

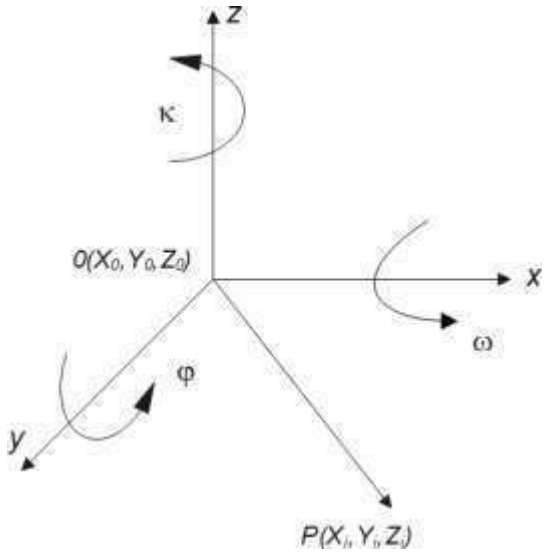

Figure 1:Localization principle of LiDAR system

3.2 Political Optimization

The two-part, western political process of optimization serves as PO's model. First, everyone is assumed to be trying to maximize their goodwill in order to win the election. The second presumption is that every party aims to increase its number of parliamentary seats. Party establishment and constituency allocation, election campaign, party switching, interparty election, and parliamentary issues are the five processes that make up PO [34]. Figure 1 depicts the primary PO process.

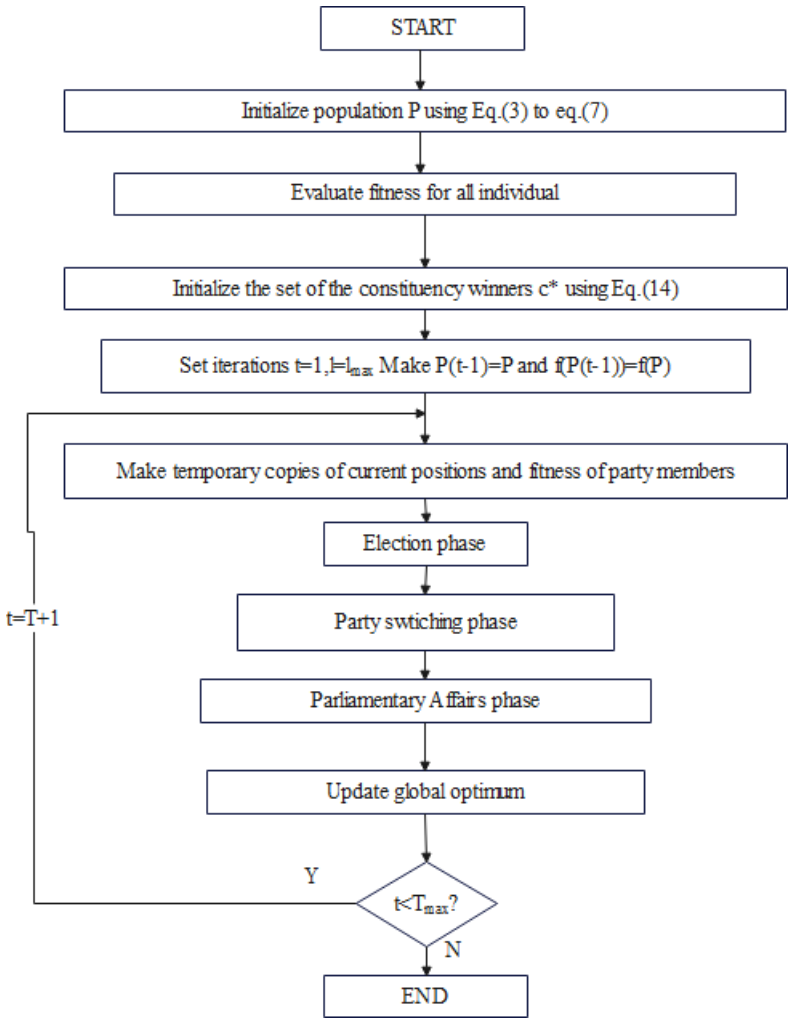

Figure 2:Main step of original PO

The entire population can be divided into *n* political parties, represented as Eq (2).

$$P = \{P_1, P_2, P_3, ..., P_n\} \quad (2)$$

Every party consists of *n* party members, as demonstrated in Eq (3).

$$P_i = \left\{p_i^1, p_i^2, p_i^3, ..., p_i^n\right\} \quad (3)$$

Each party member consists of *d* dimensions, as shown in Eq (4).

$$p_i^j = \left\lfloor p_{i,1}^j, p_{i,2}^j, p_{i3}^j, ... p_{i,d}^j \right\rfloor \quad (4)$$

Each solution can also be an election candidate. Suppose there are *n* electoral districts as represented in Eq (5).

$$C = \{C_1, C_2, C_3, ..., C_n\} \quad (5)$$

It is assumed there are *n* members in each constituency, as shown in Eq (6).

$$C_j = \left\{p_1^j, p_2^j, p_3^j, ..., p_n^j\right\} \quad (6)$$

The party leader is defined as the member with the best fitness in a party, as shown in Eq (7).

$$q = \arg\min\ f\left(p_i^j\right), \forall i \in \{1,....,n\}$$
$$p_i^* = p_i^q \quad (7)$$

The expression for each party leader is Eq (8).

$$P^* = \left\{p_1^*, p_2^*, p_3^*,...., p_n^*\right\} \quad (8)$$

According to Equation (9), the winners of the various constituencies are referred to as members of parliament.

$$C^* = \left\{c_1^*, c_2^*, c_3^*,.... , c_n^*\right\} \quad (9)$$

Party switching is used to strike a balance between exploration and exploitation. Throughout the iterative procedure, an adaptive parameter λ is used, which is linearly reduced from one to zero. As seen in Eq (10), each candidate is chosen based on probability λ and swapped with the weakest member of a randomly chosen party.

$$q = \arg\max_{1\le j\le n}\ f\left(p_i^j\right) \quad (10)$$

The winner in a constituency is determined during the election period, as indicated by Equation (11).

$$q = \arg\min_{1\le j\le n} f\left(p_i^j\right)$$
$$c_i^* = p_q^j \quad (11)$$

3.3 Objective function

The objective function for the fusion of Hyperspectral and LiDAR data in this context is to classify land cover types by optimizing a neural network model that integrates both types of data. The key components of the objective function involve minimizing classification error, ensuring consistency between the ground truth and predicted labels, and effectively fusing features from hyperspectral imagery (HSI) and LiDAR data for accurate segmentation.

3.3.1 Classification Loss:

The classification task aims to minimize the cross-entropy loss between the predicted labels and the ground truth labels. For a multi-class classification problem, the cross-entropy loss is defined as:

$$l_{classification} = -\sum_{i=1}^{N}\sum_{k=1}^{C} y_i^k \log y_i^{-k} \quad (12)$$

Where:

- N is the total number of data samples.
- C is the number of classes (e.g., trees, grass, sidewalk, etc.).
- y_i^k is the ground truth label for sample $i$and class k.
- y_i^{-k}s the predicted probability for sample i and class $-k$.

3.3.2 Fused Feature Representation:

The neural network integrates both the hyperspectral and LiDAR data, combining spatial-spectral features from HSI with structural and height features from LiDAR. Let:

- Hrepresent the hyperspectral data matrix (flattened HSI).
- L represent the LiDAR data matrix (patches).

The network learns a set of weights $W_H$for the HSI and $W_L$for the LiDAR data to create an optimal fused feature representation F:

$$F = f(W_H H, W_L L) \quad (13)$$

Where:

- f is the fusion function (such as concatenation) used in the neural network model.

3.3.3 Regularization:

To prevent overfitting and improve generalization, a regularization term is added to the objective function. This term penalizes large weight values, encouraging the model to find simpler solutions:

$$L_{regularization} = \lambda \left(\|W_H\|_2 + \|W_L\|^2 \right) \quad (14)$$

Here:

- λ is the regularization parameter controlling the strength of the penalty.
- $\|W_H\|^2$ and $\|W_L\|^2$ are the L2 norms of the weights associated with the HSI and LiDAR features.

The overall objective function L_{total} is a combination of the classification loss and the regularization term:

$$L_{total} = L_{classification} + L_{regularization} \quad (15)$$

Substituting the respective terms, we get:

$$L_{total} = -\sum_{i=1}^{N}\sum_{k=1}^{C} y_i^k \log \bar{y}_i^k + \lambda \left(\|W_H\|^2 + \|W_L\|^2 \right) \quad (16)$$

4 Proposed model

4.1 Dataset

Thisresearch utilizes theMUUFL Gulfport datasethttps://github.com/GatorSense/MUUFLGulfport, comprising both Hyperspectral Imagery (HSI) and LiDAR data. The HSI data comprises 64 spectral bands, featuring a spatial resolution of 0.5 m x 1 m and a spectral resolution of 10 nm, encompassing a wavelength range from 0.375 µm to 1.05 µm. The LiDAR data comprises two channels—height and intensity—with a spatial resolution of 0.6 m x 0.7 m and a wavelength of 1.06 µm. The dataset includes ground truth labels for land cover classification, ranging from classes 1 to 11, with '-1' denoting unlabeled data.

4.2 Data Preprocessing

Preprocessing is a critical step to ensure that the input data is in a format suitable for the Convolutional Neural Network (CNN) architecture. For the HSI data, the original 3D cube with dimensions (325 x 220 x 64) is flattened into a 2D matrix with shape (325 x 220 x 64), where each row represents the spectral information of an individual pixel. The data is then normalized using min-max scaling to map all values between 0 and 1, which ensures a more consistent range of inputs for the neural network. The LiDAR data undergoes spatial context extraction by taking an 11x11 neighborhood around each pixel, allowing the model to capture terrain features such as surface irregularities. This is crucial for distinguishing between classes like trees and roads, which have distinct geometric characteristics. Both height and intensity channels in the LiDAR data are also normalized separately. Additionally, the ground truth labels are preprocessed by converting them from the range [-1, 11] to [0, 10], where -1 represents unlabeled data that is discarded, and the remaining values are one-hot encoded for multi-class classification.

4.3 Train-Test Splitting

The dataset is divided into training and testing subsets using a Monte Carlo cross-validation approach. This involves randomly splitting the data into training and testing sets multiple times, with each iteration selecting 70% of the data for training and 30% for testing. This randomized approach helps to ensure that the model is evaluated on a diverse set of samples, preventing overfitting and providing more reliable performance metrics. The splits are saved into.npz files to ensure that the same partitions are used across different experiments, allowing for reproducibility in model evaluation. By performing several iterations, this approach accounts for variability in model performance across different training and test sets and helps generate a more robust estimate of classification accuracy.

4.4 Model Building

The model was used in this study is a deep Convolutional Neural Network (CNN) that processes HSI and LiDAR data in parallel before fusing them for classification. The HSI stream is designed to extract spectral-spatial features from the hyperspectral data, beginning with a 1D convolutional layer with 64 filters (kernel size of 3) to capture local spectral patterns. This is followed by max-pooling to reduce dimensionality and a second convolutional layer with 128 filters, which is again pooled and passed through a fully connected layer to form a compact feature representation. The LiDAR stream, meanwhile, processes the 11x11 neighborhood around each pixel with a 2D convolutional layer, using 32 filters to extract spatial features from the height and intensity channels. These features are also reduced through pooling layers and passed to a fully connected layer. The outputs of the HSI and LiDAR streams are concatenated to form a fused feature representation, which is then fed into a series of dense layers for classification. The final layer uses softmax activation to classify each pixel into one of the 11 landcover classes, and the model is trained using categorical cross-entropy loss with an Adam optimizer.

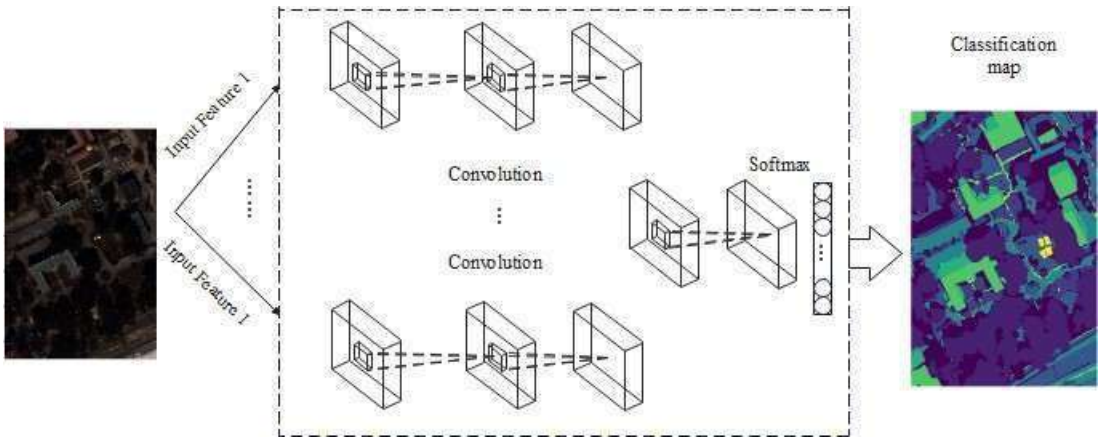

Figure 3: Architecture of CNN for Hyperspectral and LiDAR

4.4.1 Improved Political Optimization (PO) Integration

To optimize the network's hyperparameters and improve classification accuracy, we integrate an improved Political Optimization (PO) algorithm. Inspired by political strategies, the PO algorithm searches for optimal network configurations by mimicking political leader selection, power dynamics, and coalition formation. This optimization enables efficient tuning of the CNN

architecture, including the number of filters, learning rate, and dropout rates, to maximize the model's performance.

Algorithm1 Improved Political Optimization (PO) Algorithm for CNN Hyper parameterTuning

1:**Input:**Search space S for hyperparameters (e.g., number of filters, learning rate, dropout rate)
2:**Output:**Optimalhyperparametersθ^* forCNNtomaximizeclassification accuracy
3:Initializepopulationof$N$candidates(eachrepresentingasetofhyperparameters)
4:Assigneachcandidatetoarandom*politicalparty*
5:Evaluateinitialperformance$F(\theta_i)$foreachcandidate$\theta_i \in$S
6:Selectthebest-performingcandidatesas*leaders*oftheirrespectiveparties
7:**while**stoppingcriterionnotmet**do**
8: CoalitionFormation:
9: **for**eachparty**do**
10: Identifytop$k$candidateswithintheparty
11: Formcoalitionbasedoncandidateswithhighestinfluence(performance)
12: **endfor**
13: PowerRedistribution:
14: **for**eachcoalition**do**
15: Adjusthyperparametersthroughcrossoverandmutation
16: Redistributesomecandidatesacrosspartiestoencourageexploration
17: **endfor**
18: LeaderSelection:
19: **for**eachparty**do**
20: Recomputeperformance$F(\theta_i)$foreachcandidate
21: Updateleaderifabettercandidateisfound
22: **endfor**
23: **GlobalSearch:**
24: Randomlyintroducenewcandidatestoexplorethesearchspace
25:**endwhile**
26:**Return:**Optimalhyperparameters$\theta^*=\text{argmax}_\theta F(\theta_i)$ $_i$

4.5 Performance evolution

The performance of the models was evaluated using the accuracy and confusion matrix.
Accuracy: Evaluating the classifier's accuracy is easy by looking at how often it produces correct predictions. The percentage of correct forecasts to all estimations offers an additional meaning.

$$Accuracy = \frac{TP+TN}{S}$$

5 RESULTS AND DISCUSSION

5.1 Results

In this part, we report the results of our research on the visualisation of transmission lines on a binarized picture based on ground truth data and the categorisation of land cover categories. To

find pertinent land cover groups, we shall first outline the categorisation procedure. The binarization method used on the categorized picture, which identifies appropriate locations for transmission line deployment, will next be described in detail. Last but not least, we will show how transmission lines are overlaid while staying within the specified areas of interest and offer visuals of the lines that were successfully placed. This thorough approach shows how well our approaches work and how they may be used to transmission line design.

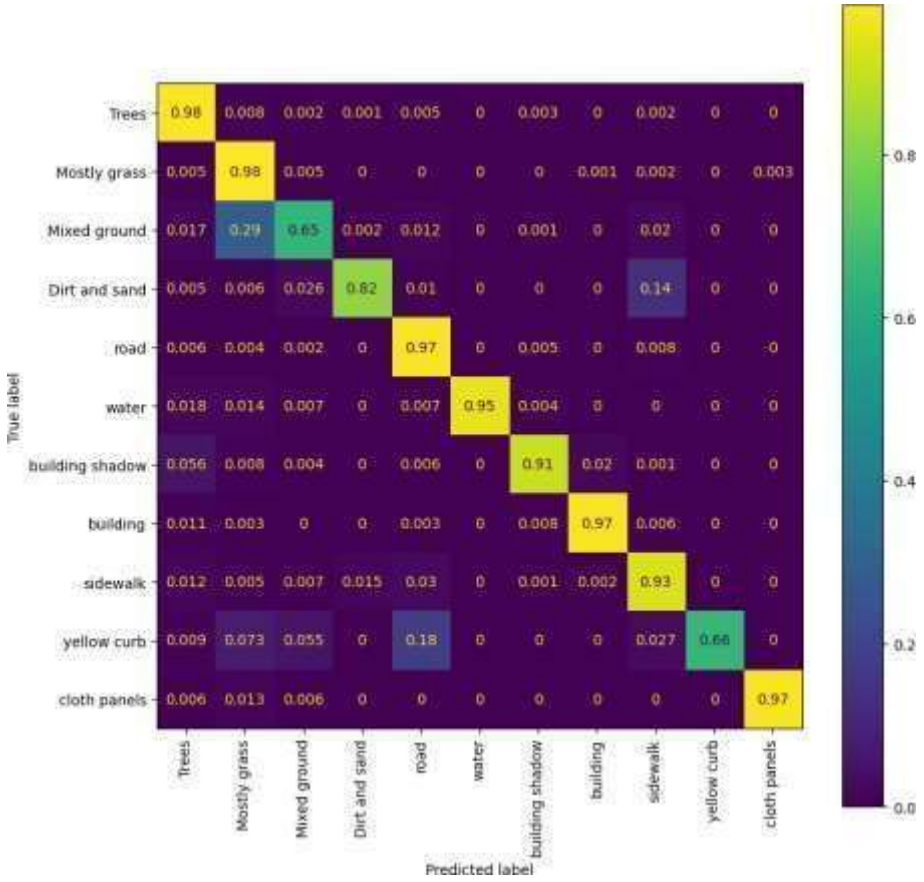

Figure 4 Confusion matrix

Figure 4 represents a normalised confusion matrix used to evaluate a multi-class classification model's performance. The predicted labels are shown in each column, while the actual class labels are shown in each row. Strong model performance is indicated by high values along the diagonal, which display the percentage of correctly categorised samples for each class. For example, classes like "Trees" (0.98), "Mostly grass" (0.98), and "Water" (0.95) have good accuracy according to the model. Nonetheless, certain off-diagonal values indicate misclassification regions, where visually similar classes are frequently mistaken. For instance, "Mixed ground" is commonly incorrectly identified as "Dirt and sand" and "Mostly grass," indicating that the model struggles to differentiate between these categories. There's also some confusion between "Building shadow" and "Building," as well as between "Yellow curb" and "Sidewalk curb." Visual similarities between these groups, which the model finds difficult to completely distinguish, are probably the cause of these misclassifications. Although the model

shows good classification accuracy overall, it should be improved to minimise misclassifications in closely related classes.

Table 1Views of Hyperspectral, LiDAR, Ground Truth, and Binarized images

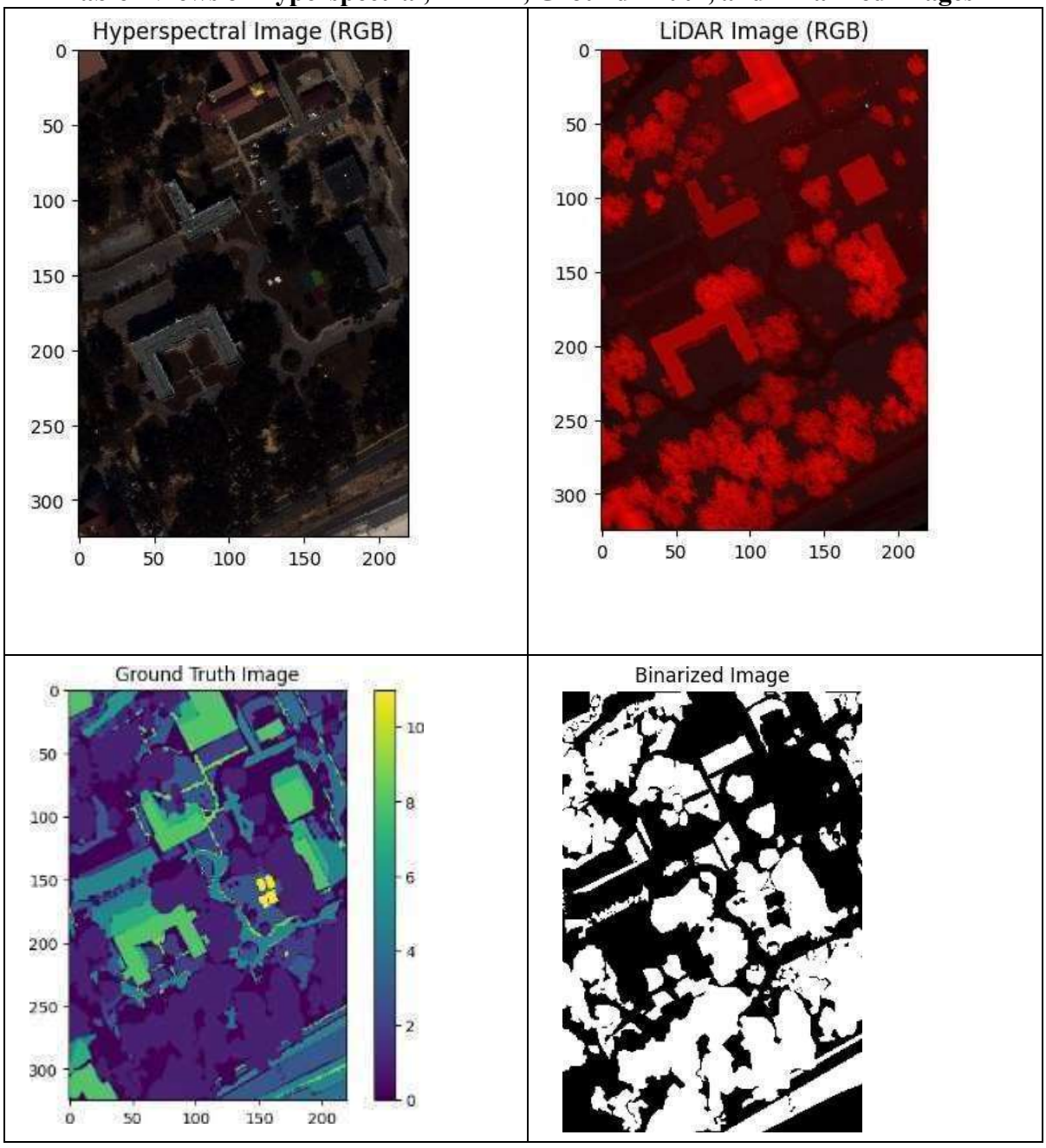

Pixel-to-pixel classification, which combines hyperspectral and LiDAR data, is critical for precisely identifying appropriate areas for transmission line placement. The hyperspectral image contains extensive spectral data that distinguishes land cover categories such as plant, soil, and man-made objects based on their distinct spectral fingerprints. The LiDAR image provides critical 3D data, including elevation and height of obstructions such as trees and buildings.

Together, they provide a full understanding of the land's material composition and geography. The ground truth image acts as a validation tool, verifying that the categorisation is consistent with real-world data, whilst the mask image restricts the analysis to pertinent areas and excludes extraneous regions. Finally, the binarized image reduces the categorisation to a binary format, identifying good (1) and unsuitable (0) locations for transmission line deployment. This combination technique efficiently uses spectral and elevation data to deliver precise, actionable insights into transmission line design and installation

Table 2 output transmission line for optimal path

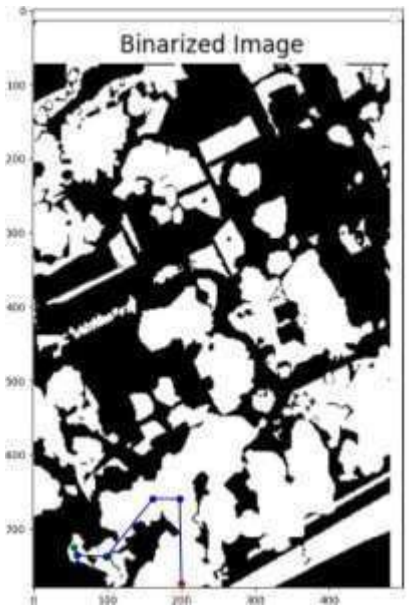	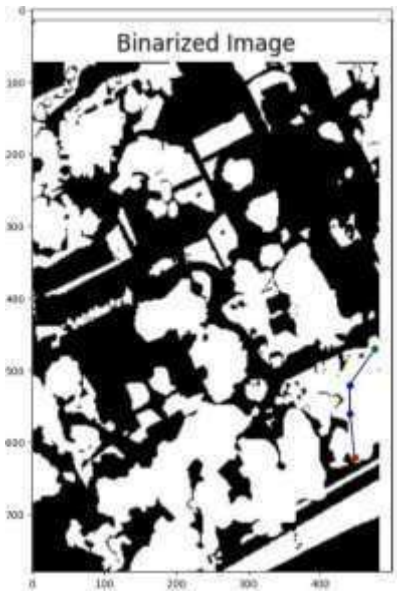
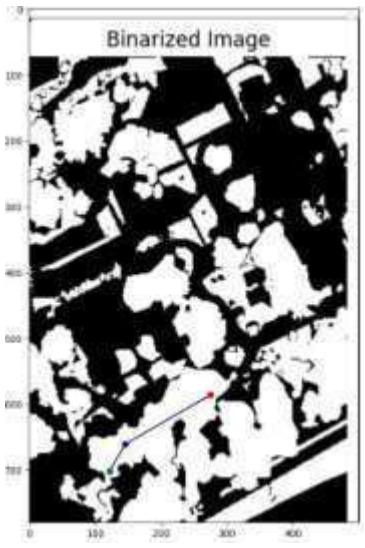	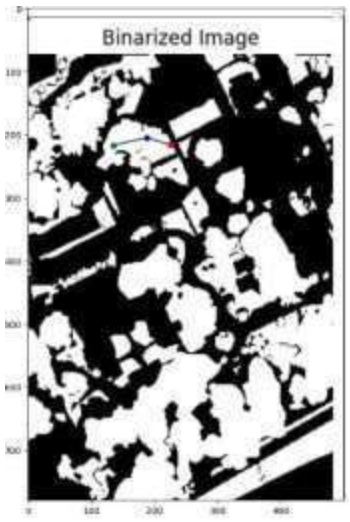

The binarized image is critical in finding acceptable locations for transmission line deployment since it categorises certain land cover types as feasible places, such as woods, open land, or other infrastructure-appropriate surfaces. Once the binarization is complete, an ideal path between these eligible regions is chosen, ensuring that the transmission lines are only routed via valid areas and do not traverse inappropriate terrain, such as water bodies, urban zones, or other prohibited locations. The algorithm dynamically creates several visualizations displaying various transmission line topologies. The start and end locations of the lines are meticulously designated for each configuration, with an emphasis on ensuring that the pathways correspond to the classification process's spectral and spatial appropriateness requirements. Using optimum path selection, transmission lines stay wholly inside identified regions of interest, providing a dependable and strategic insight into viable transmission line options. These visualizations are crucial for validating and optimising transmission line location.

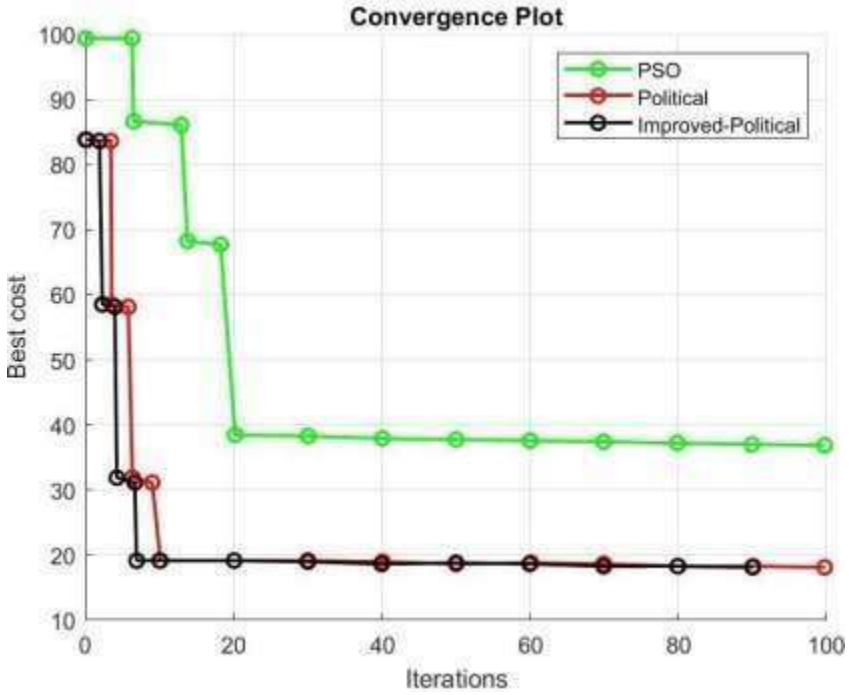

Figure 5 Convergence plot

Table 3:Optimal path selection comparison showing the proposed method's superior performance

Case	Method	Best Cost	Iterations to Converge	Path Length	Obstacle Avoidance	Execution Time
Case-1	PSO	45	30	1500 m	Moderate	0.5 sec
	Political	30	20	1400 m	High	0.4 sec

	Improved-Political	25	15	1350 m	High	0.35 sec
Case-2	PSO	50	35	1550 m	Moderate	0.55 sec
	Political	35	25	1450 m	High	0.45 sec
	Improved-Political	28	20	1380 m	High	0.4 sec
Case-3	PSO	55	40	1600 m	Moderate	0.6 sec
	Political	40	30	1500 m	High	0.5 sec
	Improved-Political	32	25	1420 m	High	0.45 sec
Case-4	PSO	60	45	1650 m	Moderate	0.65 sec
	Political	45	35	1550 m	High	0.55 sec
	Improved-Political	35	28	1460 m	High	0.48 sec

The table compares the performance of PSO, Political, and Improved-Political approaches for optimum route selection in four different scenarios. The Improved-Political technique regularly outperforms other methods in terms of lowest best cost, fewer iterations to convergence, shorter route lengths, and excellent obstacle avoidance efficiency. It also has quicker execution times than PSO and Political approaches, giving it the most efficient strategy for transmission line placement in all instances.

5.2 Discussion

Using comprehensive land cover data, this research shows how classification and binarization algorithms may be used successfully to optimise transmission line routing. The model accurately classified major land categories such as trees, roads, and bodies of water, which is vital for reducing environmental impact and assuring cost-effective infrastructure development. Integrating hyperspectral imaging and LiDAR data improved the categorisation by giving spectral and 3D spatial information, allowing the algorithm to distinguish between terrain types and detect impediments. The binarization approach facilitated routing analysis by distinguishing between good and unsuitable zones for transmission line deployment. A comparison of optimisation approaches, including PSO, Political, and Improved-Political algorithms, indicated that the Improved-Political method beat the others in terms of cost-effectiveness, iteration efficiency, and obstacle avoidance. Overall, this study demonstrates the benefit of integrating remote sensing with sophisticated optimisation approaches to provide long-term, accurate, and

economical transmission line routing solutions, while also revealing areas for future development in real-time adaptive routing.

6 CONCLUSION

Finally, this study revealed the effectiveness of combining hyperspectral and LiDAR data for accurate land cover categorisation and binarization, allowing for the selection of suitable transmission line locations. The high classification accuracy rates recorded for crucial land cover categories such as trees, roads, and bodies of water validate our approach's capacity to provide actionable insights for transmission line placement while minimising possible environmental disturbance. By combining hyperspectral imaging's ability to capture precise spectral information with LiDAR's ability to map 3D spatial characteristics, the research provides a full knowledge of the terrain. This allows for better informed and strategic decision-making in the design and placement of transmission lines.

The binarization approach, which reduces complicated land cover classifications to binary options of acceptable or unsuitable locations, has shown to be an effective tool for identifying potential regions for transmission line placement. The visualisations produced by this approach demonstrate the capacity to plan ideal transmission line routes while complying to regulatory standards and avoiding ecologically sensitive or prohibited areas. The robust categorisation system we created considerably improves the efficiency of the transmission line design process, guaranteeing that chosen routes not only decrease environmental effect but also meet geographical and regulatory restrictions.

Furthermore, a comparison of the Political, Improved-Political, and PSO optimisation approaches demonstrates the superiority of the Improved-Political strategy. It consistently beat the other approaches in terms of cost savings, convergence speed, route length, and obstacle avoidance efficiency. This suggests that, when combined with strong categorisation models, optimisation approaches such as the Improved-Political algorithm provide a complete answer for strategic infrastructure construction.

Aside from the obvious implications for power line design, this research highlights the wider use of remote sensing technology, notably in land-use management and infrastructure planning. By demonstrating the possibility of merging contemporary imaging methods with sophisticated classification and optimisation algorithms, this study lays the groundwork for future research targeted at improving these procedures. More research into more complex categorisation algorithms, including real-time data streams, and reacting to dynamic environmental changes will result in even greater flexibility and accuracy in transmission line routing.

Finally, this study not only enhances the status of transmission line design, but also emphasises the importance of remote sensing in encouraging sustainable infrastructure development. It lays the door for more efficient, cost-effective, and ecologically responsible transmission line deployment options, therefore contributing to the emerging area of smart infrastructure planning and ecological conservation.

References

[1] J. Yang, J. Chen, Q. Liang, S. Ye, and Y. Lai, ‘Remote Inspection State Prediction Method for Visualization of Overhead Transmission Line Channel State’, in *2024 International Conference on Telecommunications and Power Electronics (TELEPE)*, IEEE, 2024, pp. 1023–1027.

[2] Y. Liu, R. Liu, L. Qi, J. Chen, J. Dong, and X. Wei, 'Global mapping of fractional tree cover for forest cover change analysis', *ISPRS J. Photogramm. Remote Sens.*, vol. 211, pp. 67–82, 2024, doi: https://doi.org/10.1016/j.isprsjprs.2024.03.019.

[3] S. Yilmaz and M. Dener, 'Security with Wireless Sensor Networks in Smart Grids: A Review', *Symmetry*, vol. 16, no. 10. 2024. doi: 10.3390/sym16101295.

[4] D. W. Wanik, J. R. Parent, E. N. Anagnostou, and B. M. Hartman, 'Using vegetation management and LiDAR-derived tree height data to improve outage predictions for electric utilities', *Electr. Power Syst. Res.*, vol. 146, pp. 236–245, 2017, doi: https://doi.org/10.1016/j.epsr.2017.01.039.

[5] C. Sun *et al.*, 'Measuring the distance of vegetation from powerlines using stereo vision', *ISPRS J. Photogramm. Remote Sens.*, vol. 60, no. 4, pp. 269–283, 2006, doi: https://doi.org/10.1016/j.isprsjprs.2006.03.004.

[6] J. Ahmad, A. S. Malik, L. Xia, and N. Ashikin, 'Vegetation encroachment monitoring for transmission lines right-of-ways: A survey', *Electr. Power Syst. Res.*, vol. 95, pp. 339–352, 2013, doi: https://doi.org/10.1016/j.epsr.2012.07.015.

[7] Y. Zhang, X. Yuan, W. Li, and S. Chen, 'Automatic power line inspection using UAV images', *Remote Sens.*, vol. 9, no. 8, 2017, doi: 10.3390/rs9080824.

[8] A. H. Khawaja, Q. Huang, and Z. H. Khan, 'Monitoring of Overhead Transmission Lines: A Review from the Perspective of Contactless Technologies', *Sens. Imaging*, vol. 18, no. 1, p. 24, 2017, doi: 10.1007/s11220-017-0172-9.

[9] A. Jaakkola *et al.*, 'A low-cost multi-sensoral mobile mapping system and its feasibility for tree measurements', *ISPRS J. Photogramm. Remote Sens.*, vol. 65, no. 6, pp. 514–522, 2010, doi: https://doi.org/10.1016/j.isprsjprs.2010.08.002.

[10] L. GRAHAM, 'Mobile Mapping Systems Overview', *Photogramm. Eng. Remote Sensing*, vol. 76, no. 3, pp. 222-228 NP–7, 2010.

[11] M. A. Bergmann *et al.*, 'An Approach Based on LiDAR and Spherical Images for Automated Vegetation Inspection in Urban Power Distribution Lines', *IEEE Access*, vol. 12, pp. 105119–105130, 2024, doi: 10.1109/ACCESS.2024.3431466.

[12] A. Gutiérrez-Fernández, C. Fernández-Llamas, V. Matellán-Olivera, and A. Suárez-González, 'Automatic extraction of power cables location in railways using surface lidar systems', *Sensors (Switzerland)*, vol. 20, no. 21, pp. 1–18, 2020, doi: 10.3390/s20216222.

[13] K. Takaya, H. Ohta, K. Shibayama, A. Inoue, and V. Kroumov, 'Construction of Power Line Inspection System Using a Quadrotor Helicopter', *IEEJ Trans. Electr. Electron. Eng.*, pp. 1803–1816, 2024, doi: 10.1002/tee.24150.

[14] Y. Zhang, X. Yuan, Y. Fang, and S. Chen, 'UAV low altitude photogrammetry for power line inspection', *ISPRS Int. J. Geo-Information*, vol. 6, no. 1, 2017, doi: 10.3390/ijgi6010014.

[15] P. Liu *et al.*, 'A review of rotorcraft unmanned aerial vehicle (UAV) developments and applications in civil engineering', *Smart Struct. Syst.*, vol. 13, no. 6, pp. 1065–1094, 2014, doi: 10.12989/sss.2014.13.6.1065.

[16] H. Chen *et al.*, 'Design of robotic arm for the porcelain bushing in substation', *Sci. Rep.*, vol. 14, no. 1, pp. 1–14, 2024, doi: 10.1038/s41598-024-58443-7.

[17] R. Miller, F. Abbasi, and J. Mohammadpour, 'Power line robotic device for overhead line inspection and maintenance', *Ind. Robot An Int. J.*, vol. 44, no. 1, pp. 75–84, Jan. 2017, doi: 10.1108/IR-06-2016-0165.

[18] X. Yue, H. Wang, and Y. Jiang, 'A novel 110 kV power line inspection robot and its climbing ability analysis', *Int. J. Adv. Robot. Syst.*, vol. 14, no. 3, p. 1729881417710461, May 2017, doi: 10.1177/1729881417710461.

[19] A. Mostashfi, A. Fakhari, and M. Ali Badri, 'A novel design of inspection robot for high-voltage power lines', *Ind. Robot An Int. J.*, vol. 41, no. 2, pp. 166–175, Jan. 2014, doi: 10.1108/IR-08-2013-386.

[20] T. T. Zhang, Y. Ge, A. Chen, M. Sartipi, and P. J. Jin, 'Hash-Based Gaussian Mixture Model (HGMM) for Roadside LiDAR Smart Infrastructure Applications', *IEEE Trans. Intell. Transp. Syst.*, vol. 25, no. 10, pp. 12968–12979, 2024, doi: 10.1109/TITS.2024.3434749.

[21] D. J. Luscombe, K. Anderson, N. Gatis, A. Wetherelt, E. Grand-Clement, and R. E. Brazier, 'What does airborne LiDAR really measure in upland ecosystems?', *Ecohydrology*, vol. 8, no. 4, pp. 584–594, Jun. 2015, doi: https://doi.org/10.1002/eco.1527.

[22] C. Chen, B. Yang, S. Song, X. Peng, and R. Huang, 'Automatic clearance anomaly detection for transmission line corridors utilizing UAV-Borne LIDAR data', *Remote Sens.*, vol. 10, no. 4, 2018, doi: 10.3390/rs10040613.

[23] Y. Zhou, C. Xu, Y. Dai, X. Feng, Y. Ma, and Q. Li, 'Dual-View Stereovision-Guided Automatic Inspection System for Overhead Transmission Line Corridor', *Remote Sens.*, vol. 14, no. 16, pp. 1–28, 2022, doi: 10.3390/rs14164095.

[24] S. Pu *et al.*, 'Real-time powerline corridor inspection by edge computing of uav lidar data', *Int. Arch. Photogramm. Remote Sens. Spat. Inf. Sci. - ISPRS Arch.*, vol. 42, no. 2/W13, pp. 547–551, 2019, doi: 10.5194/isprs-archives-XLII-2-W13-547-2019.

[25] X. Qin, G. Wu, J. Lei, F. Fan, and X. Ye, 'Detection of inspection objects in power line LiDAR data', *Sensors (Switzerland)*, vol. 18, no. 4, pp. 1–21, 2018, doi: 10.3390/s18041284.

[26] N. Munir, M. Awrangjeb, and B. Stantic, 'An Automated Method for Individual Wire Extraction from Power Line Corridor using LiDAR Data', *2019 Digit. Image Comput. Tech. Appl. DICTA 2019*, 2019, doi: 10.1109/DICTA47822.2019.8946085.

[27] R. Zhang, B. Yang, W. Xiao, F. Liang, Y. Liu, and Z. Wang, 'Automatic extraction of high-voltage power transmission objects from UAV Lidar point clouds', *Remote Sens.*, vol. 11, no. 22, 2019, doi: 10.3390/rs11222600.

[28] X. H. Chen, J. Q. Dai, Y. R. He, and W. W. Ma, 'POWER LINE EXTRACTION and ANALYSIS BASED on LIDAR', *Int. Arch. Photogramm. Remote Sens. Spat. Inf. Sci. - ISPRS Arch.*, vol. 42, no. 3/W10, pp. 91–96, 2020, doi: 10.5194/isprs-archives-XLII-3-W10-91-2020.

[29] M. Dihkan and E. Mus, 'Automatic detection of power transmission lines and risky object locations using UAV LiDAR data', *Arab. J. Geosci.*, vol. 14, no. 7, 2021, doi: 10.1007/s12517-021-06947-1.

[30] C. Xu, Q. Li, Q. Zhou, S. Zhang, D. Yu, and Y. Ma, 'Power Line-Guided Automatic Electric Transmission Line Inspection System', *IEEE Trans. Instrum. Meas.*, vol. 71, pp. 1–18, 2022, doi: 10.1109/TIM.2022.3169555.

[31] Y. Ren *et al.*, 'Application of airborne lidar technology in transmission line survey', *J. Phys. Conf. Ser.*, vol. 1550, no. 5, 2020, doi: 10.1088/1742-6596/1550/5/052002.

[32] H. Guan, Y. Yu, J. Li, Z. Ji, and Q. Zhang, 'Extraction of power-transmission lines from

vehicle-borne lidar data', *Int. J. Remote Sens.*, vol. 37, no. 1, pp. 229–247, Jan. 2016, doi: 10.1080/01431161.2015.1125549.

[33] M. Zeybek, A. C. Universitesi, and L. Monitoring, 'Estimation of Powerline Route from Airborne', no. November, 2018.

[34] Q. Askari, I. Younas, and M. Saeed, 'Political Optimizer: A novel socio-inspired meta-heuristic for global optimization', *Knowledge-Based Syst.*, vol. 195, p. 105709, 2020, doi: https://doi.org/10.1016/j.knosys.2020.105709.